

Characterization of Mo Doped TiO₂ and its Enhanced Photo Catalytic Activity Under Visible Light

L. Gomathi Devi · B. Narasimha Murthy

Received: 19 May 2008 / Accepted: 28 June 2008 / Published online: 16 July 2008
© Springer Science+Business Media, LLC 2008

Abstract Transition metal doping into the TiO₂ lattice can expand the response of these metal oxide nano particles to the visible region. In view of this, Mo⁶⁺ ion is doped into the TiO₂ lattice in order to understand the mechanism of its photo response. The prepared photocatalysts were characterized by X-ray diffraction, UV–Visible absorption spectroscopy, UV–Visible diffuse reflectance spectroscopy, SEM, EDX, FTIR and BET specific surface area techniques. The characterization results have confirmed the incorporation of metal ions into TiO₂ lattice. XRD analysis shows no change in crystal structure except a slight variation in crystallite size and elongation along the *c*-axis with increase in the concentration of the dopant. Diffuse reflectance measurements showed a shift in the band edge position to longer wavelengths and an extension of the absorption to the visible region. The photo degradation efficiencies of these catalysts were studied with Tebucnazole pesticide as model pollutant. Under UV light, undoped catalyst showed higher activity than doped catalyst. But in the case of visible light irradiation Mo doped TiO₂ with intermediate dopant concentration of 0.06 atom % had the highest photocatalytic reactivity. This may be due to the narrowing of band gap so that it could effectively absorb the light of longer wavelength. The degradation path way was followed by UV–Visible spectroscopy.

Keywords TiO₂ · Mo doped TiO₂ · Tebucnazole · Visible light response · Photocatalysis · UV–Visible spectroscopy

1 Introduction

Nanostructured semiconductors in heterogeneous photo catalysis have drawn considerable attention over the past few decades. This is due to their large surface area, high Redox potential of the photogenerated charge carriers and selective reduction/oxidation of different classes of organic compounds. Among the semiconductors being studied, TiO₂ is one of the most efficient photocatalyst under UV light irradiation [1, 2]. The basic principle of semiconductor photocatalysis involves the generation electron-hole pairs which serve as redox sources. These pairs are able to initiate oxidation and reduction reactions on the TiO₂ photocatalyst [3]. The overall photo reactivity of TiO₂ is determined by various factors such as generation of charge carriers, trapping of charge carriers and rate of formation of OH radicals. In photocatalysis process electron-hole pairs are generated in femtosecond time regime which must be trapped in order to avoid recombination which takes place around 100 nanoseconds. Duration of interfacial charge transfer and charge carrier recombination is around 100 nanoseconds. The competition between these processes governs the photocatalysis. The hydroxyl ion (OH⁻) traps the valence band holes, leading to the formation of hydroxyl radicals which are strong oxidants. The adsorbed O₂ molecules acts as traps for conduction band electrons, leading to the formation of super oxide species (O₂⁻) which are unstable, reactive and may involve in several reactions [4].

Although TiO₂ is an efficient photocatalyst under UV light, many attempts have been made to study its photo response under visible light. But it is found that TiO₂ utilizes only 3–5% of the solar spectrum. Doping methods have been extensively utilized for modifying the electronic structures of TiO₂ nanoparticles to improve the photo response under solar light irradiation [5–7].

L. Gomathi Devi (✉) · B. Narasimha Murthy
Department of Chemistry, Bangalore University, Central College
Campus, Dr. Ambedkar Veedhi, Bangalore 560 001, India
e-mail: gomatidevi_naik@yahoo.co.in

When a transition metal is doped into the TiO₂ lattice, these dopants can either segregate on TiO₂ nanostructure surface or they can be incorporated into the lattice. The dopants can be substitutional, interstitial or both when incorporated. Dopants with different locations have different impact on the TiO₂ properties. It is mostly the substitutional dopant ions that contribute to the change of electronic structure and light absorption efficiency of the host. The substitutional dopant ions can induce an electronic coupling effect with the host atom and bring possible electron states within the band gap of the semiconductors [6]. The dopant related localized states on either above the valence band or below the conduction band are favorable to the band gap change, which in turn affects the photon absorption.

The location and the local bonding configuration of the dopants in TiO₂ are difficult to predict. The coordination environment of the dopants and its position is affected not only by the nature of the dopant (ionic radii and concentration) but also on the synthesis method. The quantity of dopants in the lattice will be limited by its solubility in TiO₂ lattice.

Doping of TiO₂ is done by various methods such as Ion implantation, sol-gel reaction, solid-state reaction etc., In the present research the Mo doped TiO₂ is prepared by using solid state reaction and its photocatalytic activity is studied with a pollutant tebuconazole pesticide under both UV/Solar light illumination.

Tebuconazole (TBZ) is an organo chlorine fungicide has gained renewed interest, particularly the threat of Asian soybean rust. TBZ is mainly used against diseases of turf grasses, vegetables, citrus, field crops and ornamental plants. TBZ can be applied as foliar sprays and in seed treatments. They may be applied as protectant or in curative treatments. If it is applied as a curative treatment, TBZ applications must be made early in the fungal infection process. Once the fungus begins to produce spores on an infected plant, the TBZ is not effective. Although TBZ doesn't have the degree of systemic movement like many herbicides, they are xylem-mobile. They are readily taken up by the leaves and move within the leaf. Carbon-14 labeling studies have shown that three droplets of a labeled sample of TBZ fungicide applied to a soybean trifoliolate leaf covered the entire leaf within 1 day. The TBZ is very specific in their mode of action; it inhibits the biosynthesis of sterol, a critical component for the integrity of fungal cell membrane. The brief contact with TBZ may cause slight skin irritation and redness, but inhalation of TBZ dust can cause irritation of the nose, lungs and throat. Photochemical degradation under natural sunlight is reported to be very slow in soil samples with 86% of the parent compound recovered after 34 days of irradiation. Similar inhibition effect was observed in aqueous medium [8].

The present paper focuses on the comparative study of photocatalytic efficiency of bare TiO₂ and Mo doped TiO₂ under UV/Solar light irradiation. These photo catalysts were characterized by various analytical techniques.

2 Materials and Methods

2.1 Reagents

Titanium (IV) Chloride is obtained from Merck Chemicals Ltd, (NH₄)₆Mo₇O₂₄·4H₂O from Sisco-Chem Industries, Bombay. NH₄OH, HCl, (NH₄)₂S₂O₈ and NaOH were from Sd Fine chemicals and used as supplied. Double distilled water was used for all the experiments.

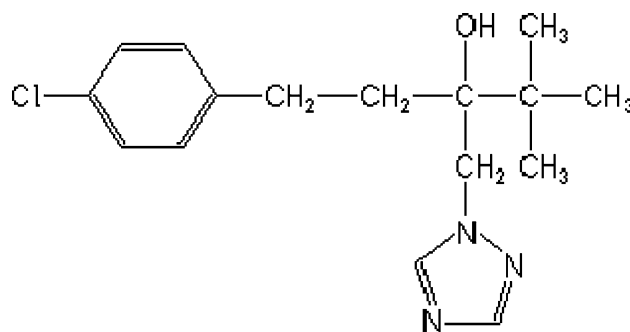
2.2 Pesticide

Tebuconazole is an organo chlorine pesticide which is obtained from an industry (pure technical grade) and used as received. The molecular weight of pesticide is 307.8, molecular formula is C₁₆H₂₂N₃ClO, IUPAC name is ((*RS*)-1-*p*-chlorophenyl-4,4-dimethyl-3-(1*H*-1,2,4-triazol-1-ylmethyl) pentan-3-ol) and its λ_{max} is 194 nm (Scheme 1).

2.3 Preparation of TiO₂ and Mo Doped TiO₂

The optically pure, fine grained anatase TiO₂ is prepared by using sol-gel method as described below.

100 mL of high purity TiCl₄ was carefully diluted by adding drop-wise to 250 mL of ice cold, well stirred double distilled water and the resulting solution was diluted to 500 mL. 25 mL of above diluted TiCl₄ made acidic by adding around 1 mL of conc. H₂SO₄ in a beaker and diluted to 1 liter with double distilled water. Liquor ammonia was added till the pH of the diluted solution attains 7–8 to obtain hydroxide of Titanium gel. The gel obtained is allowed to settle down and the gel was washed several times to remove Chloride and ammonium ions. The precipitate obtained is oven dried for 12 h at 100 °C. The oven dried TiO₂ was ground in a mortar. The fine powder



Scheme 1 Structure of tebuconazole

obtained was subject to heat treatment at 600 °C to obtain the anatase form of TiO₂ [9].

A known concentration of ammonium molybdate solution is added to TiO₂ sample to get dopant concentration of 0.02, 0.04, 0.06 and 0.1 atom percent. These mixtures were manually grinded in a agate mortar. All these samples were oven dried at 100 °C for 12 h. During the process of heating the samples were repeatedly grinded in a mortar and finally calcined at 600 °C for 4–5 h. The Stoichiometry of the prepared samples is Ti_{1-x}Mo_xO₂, where 'x' is the atom percent of Mo.

2.4 Analytical Instruments

2.4.1 X-ray Diffraction

The XRD patterns of the powders were recorded using Phillips powder diffractometer Pw/1050/70/76 with Cu K α radiation under the scan rate of 2°/min.

2.4.2 Absorption/Diffuse Reflectance Spectroscopy

The absorption and reflectance spectra were recorded by using UV–Visible Shimadzu double beam spectrophotometer 3101PC UV-VIS-NIR instrument. The spectra were recorded at room temperature in the range of 190–800 nm.

2.4.3 Scanning Electron Microscopy and Energy Dispersive X-ray Analysis

SEM was performed using a model JSM840 microscope operating at 25 kV on specimens upon which a thin layer of gold or carbon had been evaporated. An electron microprobe is used in EDX mode to obtain quantitative information on the amount and distribution of the metal species in the samples.

2.4.4 FTIR Spectral Analysis

FTIR spectra were recorded using Nicolet IMPACT 400 D FTIR spectrometer, over the range of frequencies from 4,000–400 cm⁻¹ using KBr as the reference sample.

2.4.5 Specific Surface Area Measurements

The specific surface area measurements were determined by Digisorb 2006 surface area, pore volume analyzer-Nova Quanta Chrome Corporation instrument using multipoint BET adsorption.

2.5 Photo Reactor and Light Source

Both UV and Solar illumination were used as energy sources in this study. The UV light source is a medium pressure

mercury vapor lamp and the photon flux is found to be 7.75 mW/cm² as determined by ferrioxalate actinometry, the wave length of which peaks around 340–370 nm. The photo reactor consists of a glass vessel with the exposure area of 153.86 Sq.cm. The photo degradation experiments were carried out by direct exposure of light into the reaction mixture. All the experiments were performed at room temperature in presence of atmospheric oxygen with a constant lamp power of 125 W. The distance between the photo reactor and the lamp housing is 29 cm. Experiments using solar light were carried out from 11 am to 3 pm during the summer season in the months of April–June at Bangalore, India. The latitude and longitudes are 12.58 N and 77.38 E respectively. The average sunlight intensity was found to be around 1,200 Wm⁻². The intensity of the solar light was concentrated by using a convex lens and the reaction mixture was exposed to this concentrated solar light.

The degradation path way was followed by examining the concentration of pesticide using their maximum absorbance in a UV–Visible spectrometer.

2.6 Experimental Procedure

The experiments were conducted with 250 mL of 2 ppm pesticide with 150 mg of TiO₂/Mo doped TiO₂. The reaction mixture was exposed to UV/Solar light for 150 min with constant stirring. The samples were withdrawn at regular intervals for analysis and centrifuged to separate the photo catalyst particles. The degradation path way was followed by UV–Visible Spectroscopy.

3 Results and Discussions

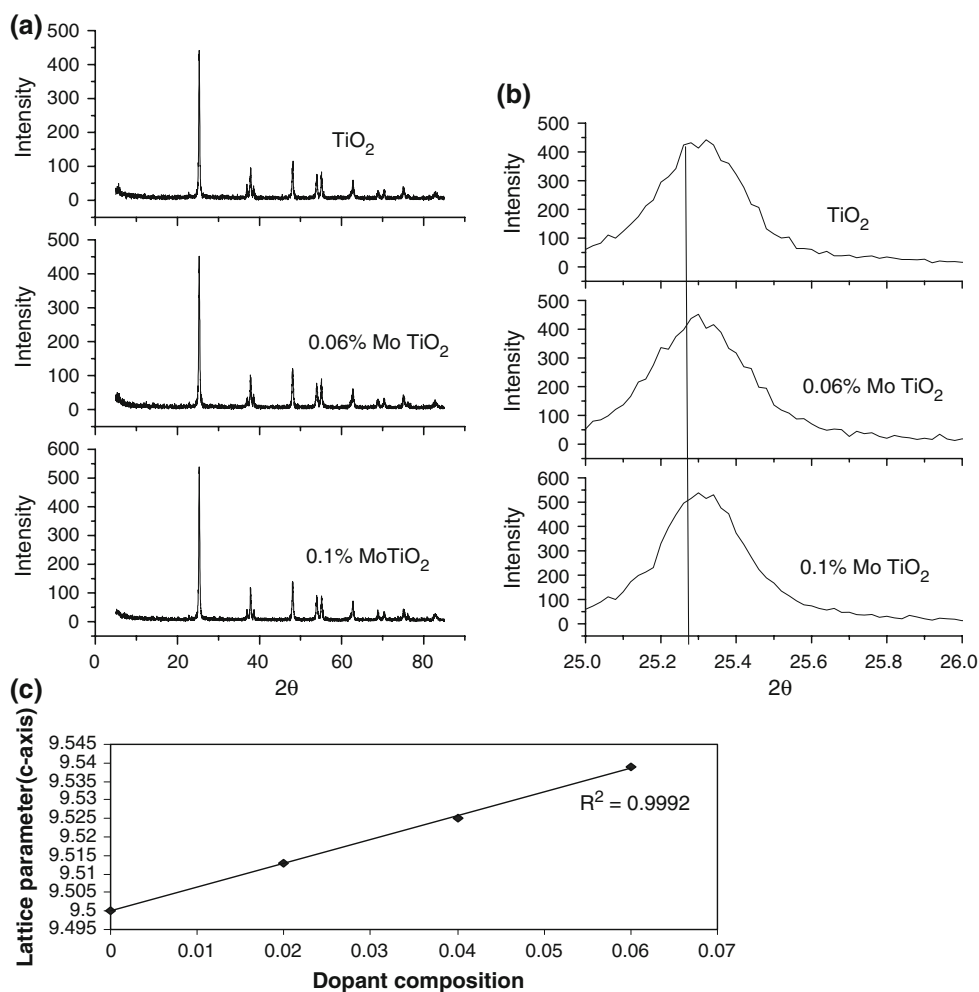
3.1 Structural Characterization of the Photo Catalysts

Catalytic properties of photo catalysts depend on its composition and structure on atomic scale. The performance of a catalyst depends on number and nature of active sites on the catalyst. Therefore the prepared catalysts were characterized by adopting following physico-chemical methods.

3.1.1 X-Ray Diffraction

Figure 1 shows the crystal structure of undoped TiO₂ and Molybdenum-doped TiO₂ as determined by X-ray diffraction. The diffraction patterns of doped powders were similar with those of pure anatase TiO₂. The average anatase crystallite size were determined by Scherer formula ($D = k\lambda/\beta\cos\theta$, where D = Crystallite size, k = share factor, λ = wavelength, θ = diffraction angle, β = Full width at half maximum) and it is found to be 26.3 nm for TiO₂ sample. The data obtained from the Scherer equation

Fig. 1 (a) XRD spectra of TiO₂ and Mo doped TiO₂ (b) XRD peak of crystal plane(101) (c) Variation of *c*-axis with dopant concentration(Vegard's law)



shows a slight increase in crystallite size with increase in Mo content. From the figure it is clear that X-ray diffraction peaks of crystal plane (101) shifts to higher diffraction angle with increase in the Mo content and hence a slight increase in crystallite size is observed (Fig. 1b). Further a change in lattice parameter corresponding to the elongation of the *c*-axis is also observed. The dopant can enter the TiO₂ lattice either interstitially or it can act as substitutional impurity. Substitution is governed by the factors like atomic size, crystal structure, electro negativity and relative valency. If these properties can match closely, substitution is possible for all compositions. In the present case the Mo is in +6 oxidation state and Ti is in +4 oxidation state. The ionic radius of Mo⁶⁺ is 0.062 nm and that of Ti⁴⁺ is 0.0605 nm. Due to the similarity in the ionic radii of Mo⁶⁺ and Mo⁴⁺ (0.068), they can replace Ti⁴⁺ in the lattice. The charge compensation is achieved mainly by the ionized vacancies especially doubly ionized oxygen vacancies. The doping Mo ion in TiO₂ lattice appears to follow Vegard's law which states that "Change in the unit cell dimension should be linear with change in the composition" This confirms the possibility of Mo substitution in TiO₂ lattice

[10]. It can be observed from the Table 1 that unit cell parameter along *c*-axis and the crystallite size keep increasing with dopant concentration up to the dispersion capacity. This linearity confirms the fact that the Mo is incorporated as substitutional dopant (Fig. 1c). The change in lattice parameters may also indicate the oxygen vacancies which are usually created along with the incorporation of impurity [11]. In the case of metal oxides there is a critical value of dispersion capacity, at values lower than which the oxide might become highly dispersed on the support without the formation of crystalline phase. Since no characteristic peaks corresponding to Mo species is present, it can be concluded that the Mo loading is below the dispersion capacity. From the XRD data, unit cell parameters, unit cell volume, crystallite size and density of all the samples is presented in Table 1.

3.1.2 UV-Visible Absorption Spectra

The UV-Visible absorption spectra of different photocatalyst nanoparticles are shown in Fig. 2. The absorption spectrum of Mo doped TiO₂ shows a red shift with increase

Table 1 Calculated structural parameters of TiO₂ and different Mo doped TiO₂ catalysts from XRD

Catalyst	2θ	d _{hkl}	Unit cell parameters (Å)	Unit cell volume (Å) ³	Crystal structure	Crystallite size (nm)	Density g/cm ³
TiO ₂	25.34	3.516	3.78	135.9	Tetragonal	26.35	3.694
	37.8	2.375	9.50				
	48.1	1.891					
0.04%Mo TiO ₂	25.3	3.512	3.78	135.7	Tetragonal	26.28	3.913
	37.8	2.378	9.51				
	48.06	1.892					
0.06%Mo TiO ₂	25.3	3.516	3.78	136.9	Tetragonal	26.30	3.877
	37.8	2.378	9.54				
	48.07	1.892					
0.1%Mo TiO ₂	25.32	3.516	3.79	136.6	Tetragonal	29.38	3.887
	37.84	2.376	9.52				
	48.12	1.892					

Density = $\frac{n \times M}{(a^2 c) N_A}$ where, n = number of atoms per unit cell, M is Molecular Mass of the catalyst, N_A = Avogadro number, a and c are lattice parameters

in the dopant concentration in the TiO₂ lattice. This may be due to the increase in the crystallite size. According to the energy band structure of TiO₂, the optical absorption in the UV range is mainly attributed to the electronic transitions from the valence band of O_{2p} to conduction band of Ti_{3d} (O_{2p} → Ti_{3d}). The optical absorption in the wavelength range 400–550 nm results from sub-band transitions closely related to the ionized oxygen vacancies [12] and also

due to the transitions from the mid band gaps formed by the Mo doping. According to the diffuse reflectance spectra the sub band levels created by ionized oxygen vacancies possibly exist below the conduction band. This may lead to different ways of electronic transitions (i) The electrons can be excited to conduction band from the top of the valence band (ii) The excitation of electrons can also take place to different levels of sub-bands related to oxygen vacancies.

Figure 2 shows the absorption band in the visible region which is mainly due to doping Mo into TiO₂ lattice. The extent and magnitude of absorbance is increases with the Mo content in the TiO₂ lattice. This may be also due to the increase in the surface oxygen vacancies amount. If the Mo⁶⁺ ion content is too high, TiO₂ would be covered with the excess Mo on the surface (deposition of the metal on the photocatalyst). This can reduce the effective area of TiO₂ surface for absorbing light. This will result in the decrease of absorbance for TiO₂ nanoparticles. Therefore, it can be predicted that photo induced charges of TiO₂ nanoparticles can be improved by doping an optimum amount of Mo⁶⁺ ions. This leads to the formation of mid band gaps in between the valence and conduction band.

The optical absorption spectra show two distinct maxima around 300–400 nm and 200–220 nm for both TiO₂ and Mo doped TiO₂ powders. These maxima corresponds to A₁ (3.59 eV) and A₂ (5.76 eV) bands reported for bulk crystals representing the electronic transition from Γ₁₅ → Γ₁₂ and Γ₂₅ → Γ₁₂ respectively [13–15]. The splitting of A₂-A₁ corresponds to 2.17 eV, this could be due to the presence of Mo⁶⁺ in TiO₂ lattice. The electronic configuration of Mo⁶⁺ is [Kr] 4d⁰ 5s⁰. Since Mo⁶⁺ does not have any valence electron, it gives extra stability to participate in electronic transitions of the doped catalyst. The introduction of energy levels by the dopants into the band gap of TiO₂ imparts color to the material. These results

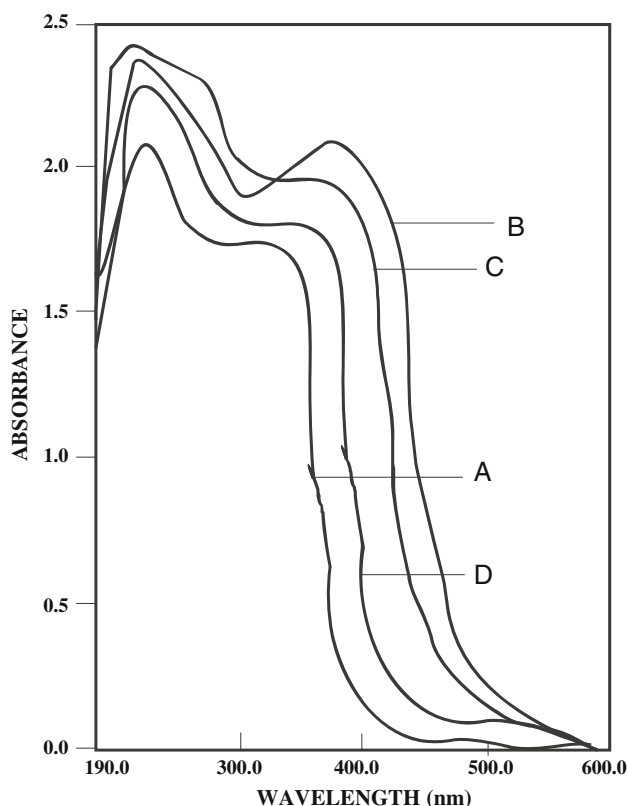


Fig. 2 Absorption spectra of the photo catalysts. (A) TiO₂, (B) 0.04% Mo doped TiO₂, (C) 0.06% Mo doped TiO₂, (D) 0.1% Mo doped TiO₂

indicate that the Mo doped TiO₂ can be a good catalyst under Visible light.

3.1.3 UV-Visible Diffused Reflectance Spectra

The reflectance data obtained was relative percentage reflectance to a non absorbing material (BaSO₄) which can optically diffuse light. P. Kubelka and F. Munk developed a theory for the diffuse reflectance of powdered samples. The Kubelka–Munk equation for an “Infinitely thick” layer is shown in Eq. 1 [16].

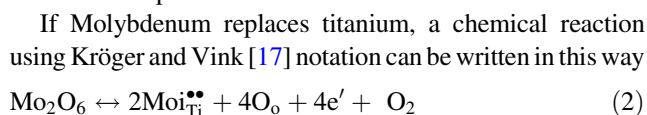
$$f(R_{\infty}) = \frac{(1 - R_{\infty})^2}{2R_{\infty}} = \frac{k}{s} \tag{1}$$

where ‘R_∞’ is the absolute reflectance of the layer, ‘s’ is the scattering coefficient and ‘k’ is the molar absorption coefficient.

The band gap energies of photo catalysts were calculated by using Kubelka–Munk plots of (1 - R_∞)²/2R_∞ versus wavelength (Fig. 3).

The band gap energies of various photo catalysts are listed in Table 2. Incorporation of various atom % of Mo

dopants into TiO₂ lattice shifts the position of its fundamental absorption edge towards the longer wavelength. In the case of 0.06% Mo doped TiO₂, the steeply diminishing region of Kubelka–Munk plot is around 480 nm, corresponds to the band gap of 2.58 eV. This absorption edge could be caused by the substitutional Mo doping. The electronic transition in undoped TiO₂ is from O-2p valence band to Ti-3d conduction band. When Mo is incorporated into TiO₂, it can dissolve inside the crystallites or settle in the grain boundaries. They can also agglomerate if the maximum solubility is exceeded. It can precipitate either at the center of crystallites or at the grain boundaries. As the mechanisms involved are complex and multiple, it is difficult to predict the exact role of dopant levels acting as active centers which are incorporated into the TiO₂ crystal lattice. Main possible reactions are shown below.



The temperature has been supposed high enough to ionize the Molybdenum atoms so that each gives up one

Fig. 3 Kubelka–Munk plots of X versus wavelength, where, X = (1 - R_∞)²/2R_∞

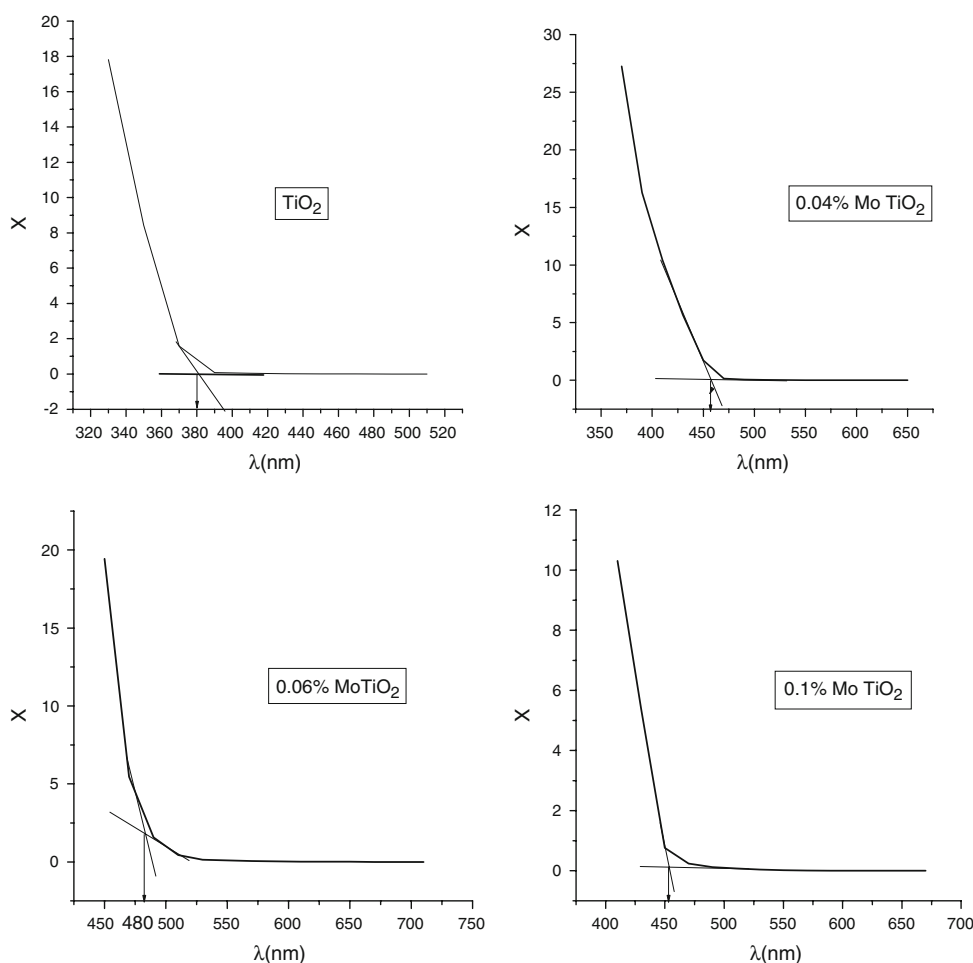
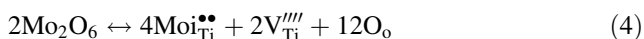
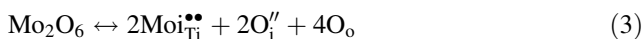


Table 2 The band gap energy for TiO₂ and Mo doped TiO₂ samples calculated from Kubelka–Munk plot

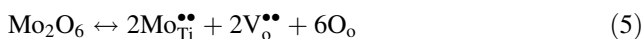
Sl. No.	Catalyst	λ (nm)	E _g (eV)
1	TiO ₂	397	3.12
2	0.04% Mo TiO ₂	440	2.81
3	0.06% Mo TiO ₂	480	2.58
4	0.1% Mo TiO ₂	450	2.75

The steeply diminishing region of diffused reflectance spectra around 400 nm corresponds to fundamental absorption edge 3.12 eV appearing for all the doped samples is not mentioned in the Table

electron. If this is not the case, the number of ionized molybdenum atoms is settled by the ionization energy at the given temperature according to Fermi-dirac distribution [18]. Instead of creating conduction band electrons, charge compensation can also be achieved by lattice defects such as interstitial oxygen's or titanium vacancies [19].



If Mo₂O₆ is dissolved substitutionally in TiO₂ and if the predominating defects are oxygen vacancies, the reaction may be written as



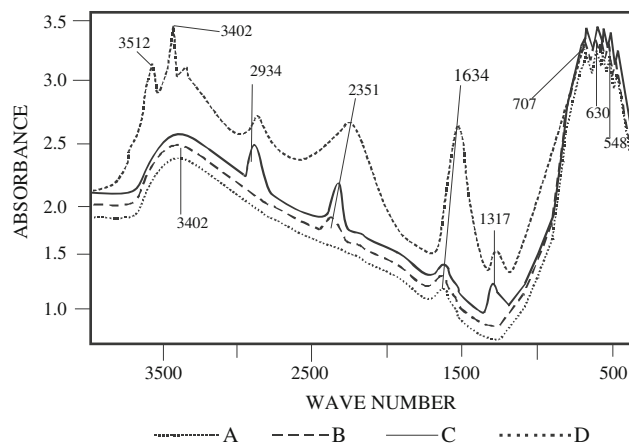
where Mo_{Ti} is a Molybdenum ion on a Titanium lattice site, V_{Ti}^{''''} is titanium vacancy (four times charged) and O_i['] is oxygen vacancy in interstitial position (two times charged), Mo_{Ti} is molybdenum ion on titanium lattice in interstitial position.

The electronic transitions in Mo doped TiO₂ may be from O-2p valence band to Mo-5d-V_o^{''} level created just below the conduction band edge by 0.58 eV. Since incorporation of certain metal ions into TiO₂ lattice is usually accompanied by vacancy in oxygen site as shown in the Eqs. 3–5. These vacancies can be singly ionized, doubly ionized or neutral. The newly created energy level below the conduction band edge at 0.58 eV with in the band gap is responsible for the activation of the catalyst under visible light illumination.

The magnitude of the reflectance increases with increase in the dopant concentration. The color of the obtained catalyst depends on the amount of the dopant into the TiO₂ lattice [20, 21].

3.1.4 SEM

The micro structural characterization of TiO₂ and Mo doped TiO₂ nanoparticles were carried out via scanning electron microscopy. Figure 4 shows the SEM image of the nanoparticles. The SEM image confirms that Mo doped TiO₂ presents a porous and sponge like network of high

**Fig. 4** SEM images of TiO₂ and Mo doped TiO₂ photo catalysts

roughness and complexity and this results in a high surface area. Further it can also be noted that particle size decreased after Mo incorporation, which results an increase in surface area for the modified systems.

3.1.5 EDX

The elemental composition of the TiO₂ and Mo doped TiO₂ samples were determined using EDX analysis and the results are listed in Table 3. From the EDX data, it is clear that theoretical atom % of the samples were very close to the experimental values. Thus by this solid state reaction it is possible to get desired loading of the metals into TiO₂ lattice.

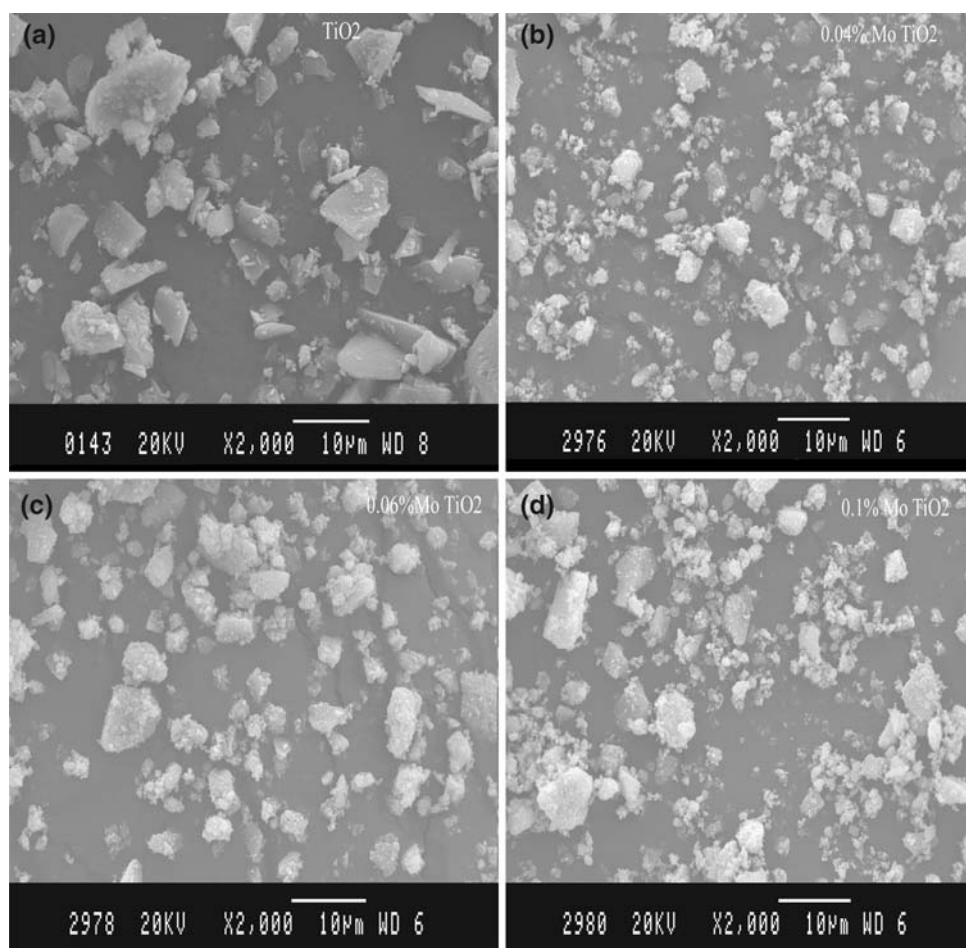
3.1.6 FTIR Absorption Analysis

The FTIR spectra of the TiO₂ and Mo doped TiO₂ samples are illustrated in Fig. 5. The spectrum of TiO₂ displays strong absorption bands at 488 and 548 cm⁻¹ which are due to the vibration of the Ti–O bond in the TiO₂ lattice [22, 23]. The peaks around 807–850 cm⁻¹ may be assigned to stretching vibration of O–O. The peak observed at 660 cm⁻¹ may be assigned to the vibration of the Ti–O–O bond [23]. The new peaks obtained at 1,317 and 2,351 cm⁻¹ for the Mo doped TiO₂ powders, can be assigned to the Mo–O vibrations. The shifting of the peaks

Table 3 EDX data for TiO₂ and Mo doped TiO₂

Sl. No.	Catalyst	Composition atom %	
		Ti	Mo
1	TiO ₂	100	–
3	0.04% Mo doped TiO ₂	96.13	5.12
3	0.06% Mo doped TiO ₂	94.34	5.66
4	0.1% Mo doped TiO ₂	90.9	11.02

Fig. 5 FTIR Spectra of the Photo catalysts (a) TiO₂, (b) 0.04% Mo doped TiO₂ (c) 0.06% Mo doped TiO₂ (d) 0.1% Mo doped TiO₂



to higher wavelengths and formation of new peaks confirms the doping of Mo into TiO₂ lattice.

The IR spectrum of OH groups in the parent TiO₂ shows band at 3,402 cm⁻¹. This peak was assigned to isolated surface hydroxyl groups [24, 25]. The band intensity of the free hydroxyl groups increases with Mo content and the wave number shifts to higher frequencies from 3,402 to 3,436 cm⁻¹. Simultaneously a peak at 2,934 cm⁻¹ appears in Mo doped TiO₂. This band is indicative of OH groups at Mo atoms on non-framework positions and represents acidic hydroxyls of varied strengths.

3.1.7 Specific Surface Area Measurements

The Nitrogen adsorption–desorption curve shows the characteristic type II isotherms (IUPAC classification) with small hysteresis loop. The surface area values are higher for Mo doped samples. Specific surface area, total pore volume, and average diameter of modified TiO₂ are summarized in Table 4. It can be observed that the surface area of the TiO₂ photocatalyst increases with the introduction of Mo into the TiO₂ lattice and the pore volume and average diameter almost remains constant for doped

samples. Therefore it can be inferred that when Mo is incorporated, the metal is homogeneously distributed in the system.

3.2 Comparative Study of Photocatalytic Activities of TiO₂/Mo Doped TiO₂ Nanoparticles Under UV/ Solar Light Illumination

3.2.1 UV Light Illumination

Photocatalytic experiments were conducted under UV light for a period of 2.5 h using TiO₂ and Mo doped TiO₂

Table 4 Surface area, pore volume and average pore diameter of the TiO₂ and Mo doped TiO₂

Sl. No.	Sample	Specific surface area (m ² /g)	Total pore volume (cm ³ /g)	Average pore diameter (Å)
1	TiO ₂ (Anatase)	18.0	0.18	89.2
2	0.02% Mo TiO ₂	24.4	0.14	203.9
3	0.06% Mo TiO ₂	28.2	0.17	205.1
4	0.1% Mo TiO ₂	23.3	0.16	251.8

Photocatalysts. The extent of degradation of the pesticide is studied by withdrawing samples for analysis at any desired time interval during irradiation. The apparent kinetics of disappearance of TBZ was followed by UV–Visible spectroscopic technique. The kinetics of disappearance of TBZ was estimated by the standard calibration curve at its λ_{\max} . The plot of C/C_0 versus Time, where C_0 is the initial concentration of the pesticide, C is the concentration of pesticide at given instant of time ‘ t ’ is shown in the Fig. 6.

From the figure it can be observed that 95% degradation of TBZ is achieved with TiO_2 in presence of $(\text{NH}_4)_2\text{S}_2\text{O}_8$ (Curve c). But in presence of TiO_2 , only 20% of degradation takes place (Curve b). Further the photo degradation of TBZ is only 5% under UV-light alone even after 6 h of irradiation. Therefore in the presence of both catalyst and Oxidizing agent the degradation is more efficient. These Oxidizing agents act as electron acceptors. They act as conduction band electron traps, which reduces the recombination rate thereby increasing the photo degradation efficiency. These acceptors are known to generate hydroxyl radicals which are thought to be the primary oxidizing species. They are known to react with aromatic hydrocarbons leading to the formation of hydroxylated derivatives and subsequent reaction of these intermediates results in complete mineralization of the pesticide.

Incorporation of Mo ion into TiO_2 lattice decreases the photocatalytic efficiency under UV light. This decrease could be explained on the basis of rate of generation of conduction band electrons and valence band holes and their life time. Usually electron hole recombination drastically

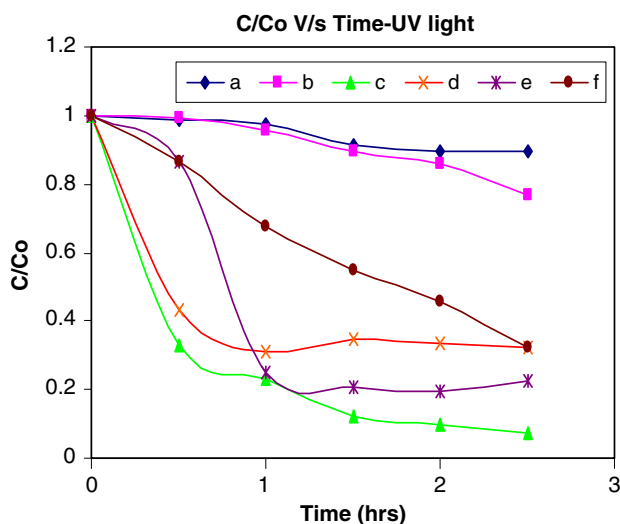


Fig. 6 C/C_0 versus Time under UV light. a—illumination of only pesticide solution, b—pesticide with only TiO_2 , c—pesticide solution with TiO_2 in presence of $(\text{NH}_4)_2\text{S}_2\text{O}_8$, d—pesticide solution with 0.04% Mo doped TiO_2 in presence of $(\text{NH}_4)_2\text{S}_2\text{O}_8$, e—pesticide solution along with 0.06% Mo doped TiO_2 and $(\text{NH}_4)_2\text{S}_2\text{O}_8$, f—pesticide solution along with 0.1% Mo doped TiO_2 and $(\text{NH}_4)_2\text{S}_2\text{O}_8$

lowers the rate of degradation. The estimated duration for electron trapping is 10 nanoseconds and holes trapping is 100 picoseconds. In the Mo ion doped TiO_2 , the mid band gaps created due to the doping may act as recombination centers under UV light [26].

Figure 7 shows the plot of $\ln C/C_0$ versus Time. The kinetic parameters like rate and order of the reaction are calculated from this plot. Higher negative slope indicates the faster rate of degradation for the experiment with TiO_2 and $(\text{NH}_4)_2\text{S}_2\text{O}_8$. Fairly good linear plots can be observed, indicating that all the reactions followed the first-order kinetics. The linear regression factor R^2 calculated for the plot $\ln C/C_0$ versus Time shows the value >0.9 suggesting the linearity of the plots except for the catalyst with higher dopant concentration.

Process efficiency, rate of the reaction, rate constant, order and the percentage of degradation of TBZ with various photo catalysts under UV illumination are shown in Table 5.

3.2.2 Solar Light Illumination

Figure 8 shows the plot of C/C_0 versus Time for various catalysts in absence of oxidizing agent under solar light irradiation. The highest photocatalytic activity was observed for the Mo doped catalyst (0.06 atom %). This may be due to the shift in the band gap to the visible region by the creation mid band gaps by the dopant. This enhances the absorption of more photons from solar light illumination. However the degradation observed was 70% for 2.5 h for the most efficient catalyst. The rate of degradation decreases thereafter. Significant increases in the degradation rate were observed by the addition of electron acceptors like $(\text{NH}_4)_2\text{S}_2\text{O}_8$. Visible light induced degradation in presence of $(\text{NH}_4)_2\text{S}_2\text{O}_8$ is presented in Fig. 9. It can be observed that only 60% of degradation of TBZ occurred in presence of TiO_2 with an oxidizing agent for 2.5 h of irradiation. But 93% degradation occurred with 0.06% Mo doped TiO_2 in presence of an oxidizing agent.

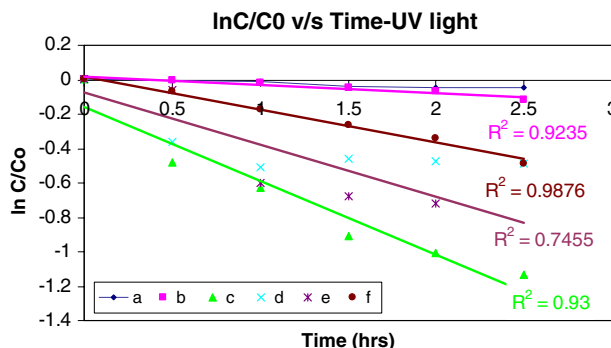


Fig. 7 $\ln C/C_0$ versus Time under UV light

Table 5 The kinetic parameters of degradation of tebuconazole under UV/solar light for 2.5 h

Exp.	UV light					Solar light				
	%D in 2.5 h	V (h ⁻¹)	η (10 ⁻⁷)	n	(k) (h ⁻¹)	%D in 2.5 h	V (h ⁻¹)	η (10 ⁻⁷)	n	(k) (h ⁻¹)
a	10	0.13	2.57	First	0.57	23	0.13	4.87	First	0.99
b	23	0.13	7.45	First	1.70	28	0.12	5.97	First	1.26
c	93	1.35	19.7	First	4.23	60	0.56	12.5	First	3.69
d	67	1.13	9.22	First	2.87	70	0.46	14.6	First	5.07
e	77	1.20	5.94	First	3.60	93	1.34	19.4	First	14.07
f	67	0.37	13.4	First	4.12	68	0.37	14.1	First	4.66

% D—percentage of degradation of pesticide, V—rate of the reaction, n—order of the reaction, k—rate constant, η—process efficiency = (C₀-C)/t × I × S, where C₀-C is decrease of pollutant concentration in mg L⁻¹, I—irradiation intensity in mwcm², S—the solution irradiated plane surface area in cm², t—the treatment time in hours

The percentage of degradation, rate constant and other parameters are listed in Table 5. It is very clear that the degradation efficiency increased with increasing the Mo content from 0.02 to 0.06 atom %. This intermediate concentration of dopant narrows the band gap and shifts the absorption band to 480 nm making the catalyst effective

for absorbing solar light. Further the degradation efficiency decreased with increase in Mo content beyond 0.06 atom %. The enhanced photo response of Mo doped TiO₂ under solar light irradiation can be accounted in the following way (i) fast interfacial electron transfer rate due to creation of new energy levels at 0.54 eV from which electron can be easily promoted to conduction band (ii) slower recombination rate of electron-holes (iii) Mo⁶⁺-V_o^{••} state is acting as electron donor below the conduction band edge.

The plot of ln C/C₀ versus (Fig. 10) shows the highest negative slope for the 0.06 atom % of Mo doped TiO₂ photocatalyst under solar light illumination, which shows the faster rate of degradation. All most all the reactions shows the linearity (linear regression factor, R² > 0.9), which indicates the first order kinetics.

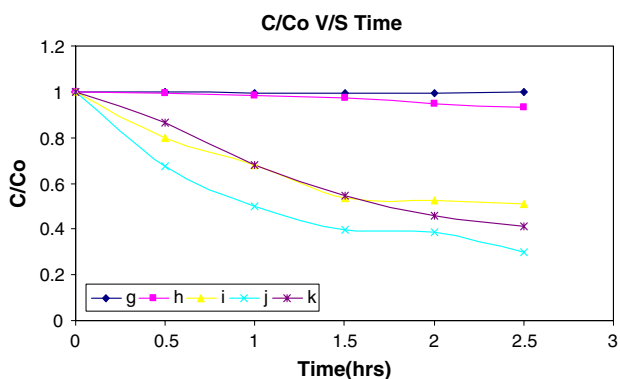


Fig. 8 C/C₀ versus Time under Solar light. g—illumination of only pesticide solution, h—pesticide with only TiO₂, i—pesticide solution with 0.04% Mo doped TiO₂, j—pesticide solution along with 0.06% Mo doped TiO₂ and (NH₄)₂S₂O₈, k—pesticide solution along with 0.1% Mo doped TiO₂

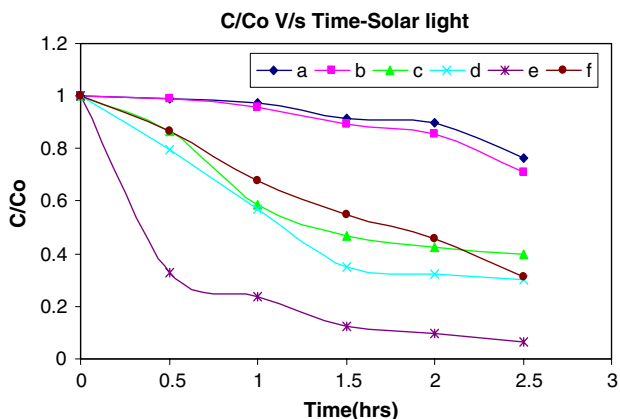


Fig. 9 C/C₀ versus Time under solar light

4 Conclusion

The doping of Mo into TiO₂ lattice is successfully achieved by solid state reaction. The samples were characterized by various analytical techniques and from the analysis the following conclusions can be drawn.

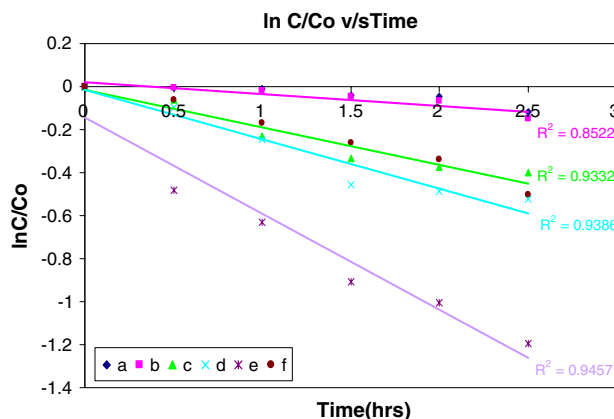


Fig. 10 ln C/C₀ versus Time under solar light

- The XRD analysis showed the increase in crystallite size and elongation along the *c*-axis with increase in the dopant concentration. The change in crystallite size and lattice parameter confirms the doping of Mo into TiO₂ lattice. In the case of doped metal oxides there is a critical value of dispersion capacity. At values lower than which the oxide might become highly dispersed on the support without the formation of a separate crystalline phase. Since no characteristic peaks corresponding to Mo species is present, it can be concluded that the Mo loading is below the dispersion capacity.
- UV–Visible absorption spectra and the diffused reflectance spectroscopic analysis showed a shift in the band gap transition to longer wavelengths and an extension of the absorption in to the visible region. The mid band gap energy level created below 0.54 eV of conduction band of TiO₂ facilitates the faster interfacial electron transfer and reduces the electron-hole recombination rate for 0.06% Mo doped TiO₂ under solar light. This accounts for the enhanced photo response of doped TiO₂ under visible region.
- The peaks obtained at 1,317 and 2,351 cm⁻¹ in FTIR confirms the presence of Mo in TiO₂ matrix. These peaks may be assigned for the Mo–O vibrations.
- The comparative study of photocatalytic activity of TiO₂ and Mo doped TiO₂ shows the faster degradation of tebuconazole pesticide with TiO₂ in presence of UV light. Further an appropriate amount of Mo (0.06 atom %) dopant enhanced the photo catalytic activity of Mo doped TiO₂ under visible light irradiation. Most of the photocatalytic reactions followed the first order kinetics.

Acknowledgements Financial support by UGC-Major Research Project (2007–2010), UGC-DRS, and UGC-FIST is greatly acknowledged. One of the author B. Narasimha Murthy wishes to acknowledge CMR Institute of Technology, Bangalore for its support.

References

1. Pelizzetti E, Serpone N (eds) (1986) Homogeneous and heterogeneous photocatalysis. Reidel, Dordrecht
2. Schiavello M (1988) Photocatalysis and environment. Trends and applications. Kluwer Academic Publishers, Dordrecht
3. Fujishima A, Rao TN, Tryk DA (2000) J Photochem Photobiol C: Photochem Rev 1:1–21
4. Augugliaro V, Loddo V, Marchi G, Palmisano L, lopezmunoz MJ (1997) J Catal 166:272
5. Guha S, Ghosh K, Keeth JG, Ogale SB, Shinde SR, Simpson JR, Drew HD, Venkatesan T (2003) Appl Phys Lett 83:3296
6. Weng HM, Yang XP, Dong JM, Mizuseki H, Kawasaki M, Kawazoe Y (2004) Phys Rev B 69:125219
7. Matsumoto Y, Murakami M, Shono T, Hasegawa T, Fukumura T, Kawasaki M, Ahmet P, Chikyow T, Koshihara S, Koinuma H (2001) Science 291:854
8. Katagi T (2004) Rev Environ Contam Toxicol 182:1–195
9. Gomathi Devi L, Krishnaiah GM (1999) J Photochem Photobiol A: Chem 121:141–145
10. Azaroff LV (1977) Introduction to solids, TMH edn. McGraw-Hill Inc., New York
11. Prasad K, Bally Philippe AR, Schmid E, Lévy F, Benoit J, Barthou C, Benalloul P (1997) J Appl Phys 36:5696–5702
12. Lee JD (1996) Concise inorganic chemistry, 5th edn. Chapman and Hall Publication, London
13. Kutty TRN, Gomathi Devi L (1985) Mater Res Bull 20:793
14. Fuller MP, Griffiths PR (1978) Anal Chem 50(13):1906–1910
15. Cardona M, Harbeke G (1964) Phys Rev 137A:1467
16. Fuller MP, Griffiths PR (1978) Anal Chem 50(13):1906–1910
17. Kröger FA, Vink HJ (1956) Solid state physics. Academic Press, New York
18. Bernasik A, Radecka M, Rekas M, Sloma M (1993) Appl Surf Sci 65:240
19. Mizushima K, Tanaka M, Asai A, Iida S, Goodenough JB (1979) J Phys Chem Solids 40:1129
20. Suda Y, Kawasaki H, Ueda T, Ohshima T (2004) Thin Solid Films 453–454:162
21. Wawrzyniak B, Morawski AW, Tryba B (2006) Int J Photoener 2006:1–8
22. Yoko XT, Kamiya K, Tanaka K (1990) J Mater Sci 25:3922
23. Zhang J, Boyd I, Sullivan BJO, Hurley PK, Kelly PV, Senateur JP (2002) J Non-Cryst Solid 303:134
24. Yamakata A, Aki Ishibashi T, Onishi H (2002) Bull Chem Soc Jpn 75:1019
25. Jackson P, Parfitt GD (1971) Trans Faraday Soc 67:2469
26. Maruska HP, Ghosh AK (1979) Solar Energy Mater 1:237